Matthew D. Fronk
School of Mechanical Engineering,
Georgia Institute of Technology,
Atlanta, GA 30332
e-mail: mfronk3@gatech.edu

Sameh Tawfick
Assistant Professor
Department of Mechanical Science and Engineering,
University of Illinois, Urbana—Champaign,
Urbana, IL 61801
e-mail: tawfick@illinois.edu

Chiara Daraio
Professor
Division of Engineering and Applied Science,
California Institute of Technology,
Pasadena, CA 91125
e-mail: daraio@caltech.edu

Shuangbao Li
College of Science,
Civil Aviation University of China,
Tianjin, China
e-mail: shuangbaoli@yeah.net

Alexander Vakakis
Professor
Department of Mechanical Science and Engineering,
University of Illinois, Urbana—Champaign,
Urbana, IL 61801
e-mail: avakakis@illinois.edu

Michael J. Leamy[1]
Professor
School of Mechanical Engineering,
Georgia Institute of Technology,
Atlanta, GA 30332
e-mail: michael.leamy@me.gatech.edu

Acoustic Non-Reciprocity in Lattices With Nonlinearity, Internal Hierarchy, and Asymmetry: Computational Study

Reciprocity is a property of linear, time-invariant systems whereby the energy transmission from a source to a receiver is unchanged after exchanging the source and receiver. Nonreciprocity violates this property and can be introduced to systems if time-reversal symmetry and/or parity symmetry is lost. While many studies have induced nonreciprocity by active means, i.e., odd-symmetric external biases or time variation of system properties, considerably less attention has been given to acoustical structures that passively break reciprocity. This study presents a lattice structure with strong stiffness nonlinearities, internal scale hierarchy, and asymmetry that breaks acoustic reciprocity. Macroscopically, the structure exhibits periodicity yet asymmetry exists in its unit cell design. A theoretical study, supported by experimental validation, of a two-scale unit cell has revealed that reciprocity is broken locally, i.e., within a single unit cell of the lattice. In this work, global breaking of reciprocity in the entire lattice structure is theoretically analyzed by studying wave propagation in the periodic arrangement of unit cells. Under both narrowband and broadband excitation, the structure exhibits highly asymmetrical wave propagation, and hence a global breaking of acoustic reciprocity. Interpreting the numerical results for varying impulse amplitude, as well as varying harmonic forcing amplitude and frequency/wavenumber, provides strong evidence that transient resonant capture is the driving force behind the global breaking of reciprocity in the periodic structure. In a companion work, some of the theoretical results presented herein are experimentally validated with a lattice composed of two-scale unit cells under impulsive excitation. [DOI: 10.1115/1.4043783]

Keywords: nonreciprocity, periodic structures, nonlinear wave propagation, hierarchical materials

1 Introduction

Reciprocity exists in linear time-invariant (LTI) acoustic, elastic, thermal, and electrostatic systems, wherein a source transfers energy to a receiver, and the same energy would also transfer back should the locations of the source and receiver be exchanged. Mathematically, it corresponds to symmetric Green's functions and self-adjoint operators [1]. In a broader context, in LTI (possibly inhomogeneous) waveguides, acoustic reciprocity is directly related to time-reversal symmetry through the *Onsager-Casimir principle of microscopic reversibility* [2–4]. Accordingly, *breaking of reciprocity in LTI acoustics is only possible by breaking time-reversal symmetry on the microlevel* [5], but not necessarily on the macrolevel; e.g., in linear absorbing media, although time-reversal symmetry is broken in the macrolevel, reciprocity still holds since time reversibility at the microlevel is preserved. Note that time-reversal symmetry here is different with just reversing (i.e., going back in) time [6]; e.g., in a system with viscous damping going back in time, the energy reverses back to the system and entropy decreases; in that sense, any deterministic system has this symmetry. True breaking of time-reversal symmetry yields asymmetrical wave propagation and, hence, is directly linked to acoustic nonreciprocity. For example, in a one-dimensional (1D) acoustic medium excited at its center, a wave propagating asymmetrically suggests that the locations of a source and receiver cannot be exchanged without expecting a difference in the measured response: waves propagate rightward in a fundamentally different manner than leftward.

Many studies have reported nonreciprocity in systems with odd-symmetric external biases, or some active external force that biases the direction of energy transmission. Such external biases range from magnetic fields in electrical systems [7] to circulating fluid flow in acoustic systems [8] to moving, zero-index acoustic metamaterials [9]. Additional active methods of breaking reciprocity include space/time modulation of material properties which has received increasing intention in recent years. By periodically varying density and Young's modulus, Trainiti and Ruzzene [10] reported large disparities in opposite directions of band diagrams, from which the optimal modulation speed for maximizing nonreciprocity was derived. In Ref. [11], harmonic spatiotemporal modulation of density and modulus in periodic laminates produces asymmetric propagation for supersonic and subsonic modulation

[1]Corresponding author.

Contributed by the Technical Committee on Vibration and Sound of ASME for publication in the Journal of Vibration and Acoustics. Manuscript received January 23, 2018; final manuscript received April 29, 2019; published online June 11, 2019. Assoc. Editor: Mahmoud Hussein.

speeds. In the scale-separated homogenization limit, the Willis stress–velocity momentum–strain coupling tensor provides a direct measurement of the nonreciprocity. A comprehensive dispersion analysis of modulating material properties in two-dimensional phononic crystals is provided in Ref. [12]. Photon–phonon conversion [13], activation/deactivation of periodically spaced electrodes [14], and magnetically active elastic materials [15] are other recent efforts of breaking reciprocity through modulation of a medium's properties.

Considerably less attention has been given to systems that passively break reciprocity—particularly within the acoustics community. Liang et al. [16,17] developed an acoustic rectifier by coupling a linear superlattice to a nonlinear medium and exploiting the bandgaps of the superlattice and the higher harmonic generation of the nonlinear medium to induce nearly one-way wave propagation. A similar study was carried out by Luo et al. [18] in which linear and nonlinear lattices with identical masses were joined at an interface. A shift in the acoustic branch but not in the optical branch occurred, enabling a bias in propagation direction at sufficiently high amplitudes. Boechler et al. [19] experimentally observed acoustic rectification by similar means in a granular chain with a point defect. In both studies, the location of the interface or the defect relative to the source of excitation limits the application of the designs for sound and vibration isolation and furthermore requires the "upconverting" of the wave at its fundamental frequency to higher harmonics, thus not retaining all signal information. In another study [20], reciprocity was passively broken in a metastable chain, and dispersion analysis of the nonreciprocal wave propagation was reported.

Local nonreciprocity in a unit cell with a two-scale internal hierarchy was presented in Ref. [21], in which energy preferably transfers from a large scale to a small scale via a purely nonlinear coupling. Transient resonance capture (TRC) was identified as the primary dynamical mechanism governing this phenomenon, linked to a critical level of energy in the system and the essentially nonlinear spring coupling the two scales. Experimental validation of local nonreciprocity in the two-scale unit cell under impulsive excitation was also reported in Ref. [22].

This study builds upon the hierarchical structure reported in Ref. [21] by extending it to a periodic configuration with inherent asymmetry in its coupling of unit cells. First, a review is provided detailing the manner in which internal hierarchy and nonlinearity induce nonreciprocity in a single isolated unit cell. Transient resonance capture is presented as the underlying mechanism governing the local nonreciprocity. Informed by these results, particularly that transient resonance capture is activated at certain energy levels, analysis of global nonreciprocity in the periodic system is presented herein. "Giant" breaking of reciprocity in the 1D chain of unit cells subjected to narrowband and broadband excitation is reported. The results of varying impulse amplitude, harmonic forcing amplitude, and frequency/wavenumber provide strong evidence that transient resonance capture drives the global breaking of reciprocity in the lattice.

2 System Description

The proposed structure consists of a chain of unit cells containing an arbitrary number of nested springs, masses, and dampers. An isolated single unit cell of this periodic structure is presented in Fig. 1. In this particular example, the unit cell contains three scales: an outer mass (the large scale) is grounded via a linear spring and couples, via a purely cubic spring, to a smaller mass (the intermediate small scale) nested within it, which in turn couples by another purely cubic spring to a still smaller mass (the smallest scale). Linear dampers are included in parallel with all springs. The extension to multiple nested layers (and hence internal hierarchies of multiple, continuously decreasing small scales) is straightforward. While the spring-mass-damper configuration is shown at the right, a proposed concept for constructing the structure is shown at the left, in which the pyramids represent elastomeric bumpers that are

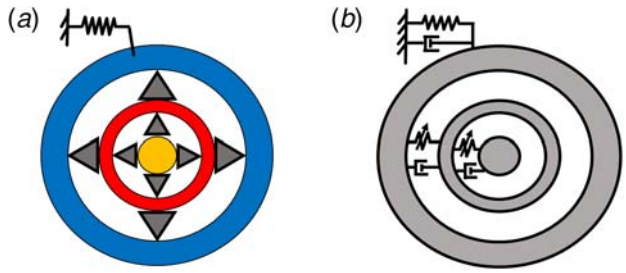

Fig. 1 Isolated unit cell of the asymmetrical, hierarchical lattice structure: (*a*) proposed fabrication method in which nonlinear coupling is achieved by elastomeric bumpers and (*b*) the equivalent spring-mass-damper model of the unit cell

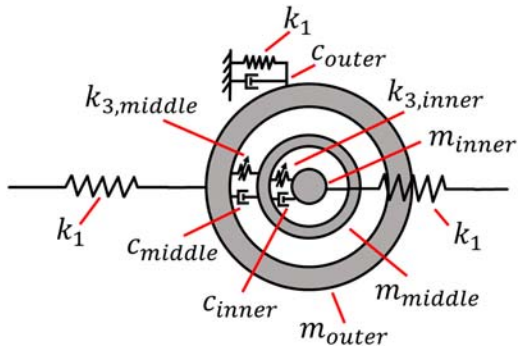

Fig. 2 Hierarchical unit cell with labeled parameter notation

Table 1 Sample normalized parameter values for the hierarchical unit cell

Parameter	Value
m_{outer}	1
m_{middle}	0.05
m_{inner}	0.005
k_1	1
$k_{3,middle}$	1
$k_{3,inner}$	0.1
c_{outer}	2E-03
c_{middle}	2E-03
c_{inner}	2E-04

known to provide near-cubic restoring forces in compression [23–25]. Normalized parameter values are chosen such that they scale down at each layer of the unit cell. A labeled schematic is presented in Fig. 2 and a sample set of parameter values is given in Table 1.

The hierarchical structure is repeated periodically to form a lattice as shown in Fig. 3. Note that the smallest mass in the unit cell is coupled to the largest mass of its right-neighboring unit cell via a linear spring. Thus, this periodic arrangement exhibits the requisite asymmetry.

3 Local Nonreciprocity Study

Analysis of a single unit cell consisting of only two scales is first reviewed in this section, detailing the findings in Ref. [21] as well as presenting new results on the effect of varying the normalized parameters on the local nonreciprocity. Two scales are considered to reduce the complexity of this isolated unit cell analysis and present the basic principles governing the global system. However, this analysis extends to any number of nested scales. Figure 4 presents a dynamical model of this isolated unit cell with labeled coordinates and parameter names.

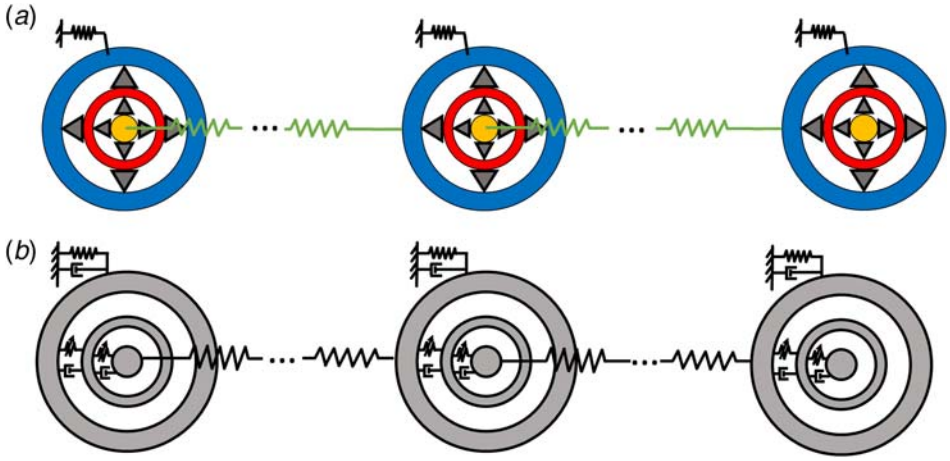

Fig. 3 Lattice structure containing unit cells with internal hierarchy, nonlinearity, and asymmetry: (*a*) the elastomeric bumper design is extended periodically and (*b*) spring-mass-damper representation of the lattice

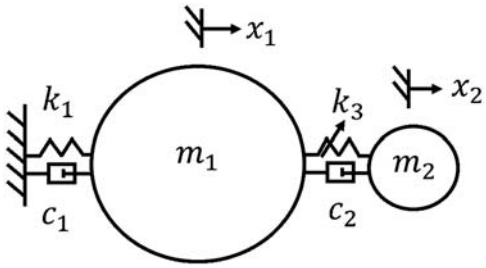

Fig. 4 Hierarchical unit cell consisting of two scales

The equations of motion governing this system are

$$m_1\ddot{x}_1 = -k_1x_1 - k_3(x_1 - x_2)^3 - c_1\dot{x}_1 - c_2(\dot{x}_1 - \dot{x}_2) \tag{1}$$

$$m_2\ddot{x}_2 = k_3(x_1 - x_2)^3 + c_2(\dot{x}_1 - \dot{x}_2) \tag{2}$$

To investigate nonreciprocity, the response of this system to impulses at either the large scale (LS) or small scale (SS) is simulated by direct numerical integration of the equations of motion, with the aim of measuring the steady-state distribution of energy when either scale is excited. To model the impulses, nonzero initial velocities are assigned to the desired scale of the form

$$V_0 = \frac{I_0}{m_n} \tag{3}$$

where V_0 denotes the initial velocity, m_n the desired scale to excite ($n = 1$ or 2 for LS or SS excitation, respectively) and I_0 is the total momentum, or impulse magnitude, imparted into the system. For a fair comparison of the system's response when either scale is excited, I_0 remains constant.

To track the energy distribution in the system, a dimensionless parameter $E_{D,SS}$ is defined

$$E_{D,SS} = \lim_{T\to\infty} \frac{\int_0^T c_2(\dot{x}_2(t) - \dot{x}_1(t))^2 dt}{\frac{1}{2}m_nV_0^2} \tag{4}$$

where again $n = 1$ or 2 for LS or SS excitation, respectively. This dimensionless parameter is the steady-state fraction of system energy that is dissipated by the damper coupling of the two scales. The limit imposes that T should be large enough for the system energy to dissipate and $E_{D,SS}$ to converge. By examining $E_{D,SS}$, the distribution of impulse energy over the course of the simulation can be assessed for both LS and SS excitations.

Impulse magnitudes I_0 are varied and $E_{D,SS}$ computed for both LS and SS excitations, and the results are presented in Fig. 5. When $0.1 < I_0 < 0.7$, the system energy transfers from the LS to the SS when the LS is excited; however, energy remains confined at the SS for all the impulse magnitudes shown. *Thus, reciprocity is broken locally.*

The underlying mechanism behind this local breaking of reciprocity is elucidated by analyzing the dynamics of the two-scale system in the frequency domain. For the LS excitation, the SS quickly "tunes" its frequency via 1:1 TRC to oscillate near the LS natural frequency. The innermost mass and essentially nonlinear spring have no predefined natural frequency, but rather can match the instantaneous natural frequency of the LS assuming it has enough energy. Thus, the impedance mismatch of the two oscillators rapidly minimizes and energy efficiently transmits, or "pumps" from the LS to the SS where it is then dissipated by the damper coupling the two scales. TRC is activated only at certain energy levels: when the initial momentum delivered to the system is too low, TRC is not activated and the response is considerably more reciprocal. When the SS is excited, it does not immediately oscillate at the LS natural frequency. Rather, the essentially nonlinear spring produces various frequencies at which the SS vibrates until the SS finally settles upon the LS natural frequency. By the time the SS reaches this frequency for efficient energy transfer, most of the system energy has been dissipated by the damper coupling the two scales. Thus, the energy remains *localized* at the SS instead of transferring to the LS as would be expected in a linear, time-invariant system. Additional analysis of the TRC phenomenon in this system can be found in Ref. [21].

Insight into the TRC is aided by the variable transformation

$$y_1 = x_1 + \varepsilon x_2, \quad y_2 = x_1 - x_2 \tag{5}$$

where y_1 and y_2 represent the motion of the center of mass (ε is the ratio of the small mass to the large mass) and the relative stretch in the system, respectively. Note that because of the scaling inherent to the hierarchical structure, $\varepsilon \ll 1$ and thus $y_1 \approx x_1$ and $y_2 \approx x_2$. These physical coordinates can readily be transformed into action-angle variables (I_1, θ_1) and (I_2, θ_2) [21]

$$I_1 = \frac{1}{2}(y_1^2 + \dot{y}_1^2), \quad \theta_1 = \cos^{-1}\left(\frac{y_1}{\sqrt{2I_1}}\right), \quad I_2 = \left[\frac{\dot{y}_2^2\pi^2}{2K^2(1/2)\Lambda^2\Xi^2} + \frac{y_2^4}{\Lambda^4}\right]^{\frac{3}{4}}$$
$$\mathrm{cn}\left[\frac{2K(1/2)\theta_2}{\pi}, \frac{1}{2}\right] = \frac{y_2}{\Lambda I_2^{\frac{1}{3}}} \tag{6}$$

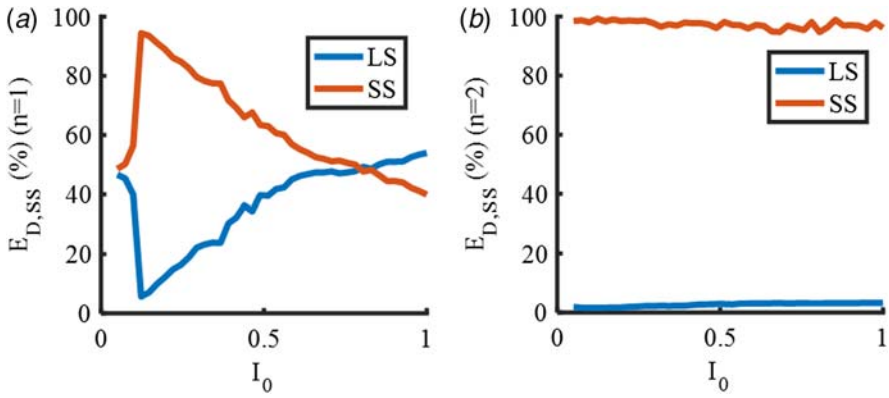

Fig. 5 Response of the two-scale system to different impulse magnitudes: (*a*) LS excitation and (*b*) SS excitation

where

$$\Lambda = \left(\frac{1}{4}\right)^{\frac{1}{6}}\left(\frac{3\pi}{K(1/2)}\right)^{\frac{1}{3}}, \quad \Xi = \left(\frac{3\pi^4}{8K^4(1/2)}\right)^{\frac{1}{3}} \tag{7}$$

and I_1, I_2 and θ_1, θ_2 denote the action and angle variables, respectively, $K(1/2)$ the complete elliptic integral of the first kind parameterized by $m = 1/2$, and $\mathrm{cn}[u, m]$ denotes the Jacobi elliptic function evaluated at u and parameterized by m. The action variables I_1 and I_2 relate to the instantaneous energies of y_1 and y_2, respectively, whereas the angle variables θ_1 and θ_2 relate to the phase of oscillation of y_1 and y_2, respectively.

When designing unit cells to break reciprocity, it is important to predict the system's response under different parameter sets (i.e., mass, stiffness, damping values). To explore this effect, the equations of motion in Eqs. (1) and (2) can be nondimensionalized [21]

$$q_1'' + q_1 + \Pi_{c_1} q_1' + \Pi_{k_3}(q_1 - q_2)^3 + \Pi_{c_2}(q_1' - q_2') = 0 \tag{8}$$

$$\Pi_m q_2'' + \Pi_{k_3}(q_2 - q_1)^3 + \Pi_{c_2}(q_2' - q_1') = 0 \tag{9}$$

where

$$x_n(t) = \alpha q_n(\tau), \quad \tau = \omega_0 t, \quad \omega_0^2 = \frac{k_1}{m}, \quad \Pi_{c_1} = \frac{c_1\omega_0}{k_1}, \quad \Pi_{c_2} = \frac{c_2\omega_0}{k_1}, \quad \Pi_m = \frac{m_2}{m_1}, \quad \Pi_{k_3} = \frac{k_3\alpha^2}{k_1} \tag{10}$$

and $()'$ denotes differentiation with respect to the dimensionless time τ. The parameter α is the scale of the unit cell's deformation

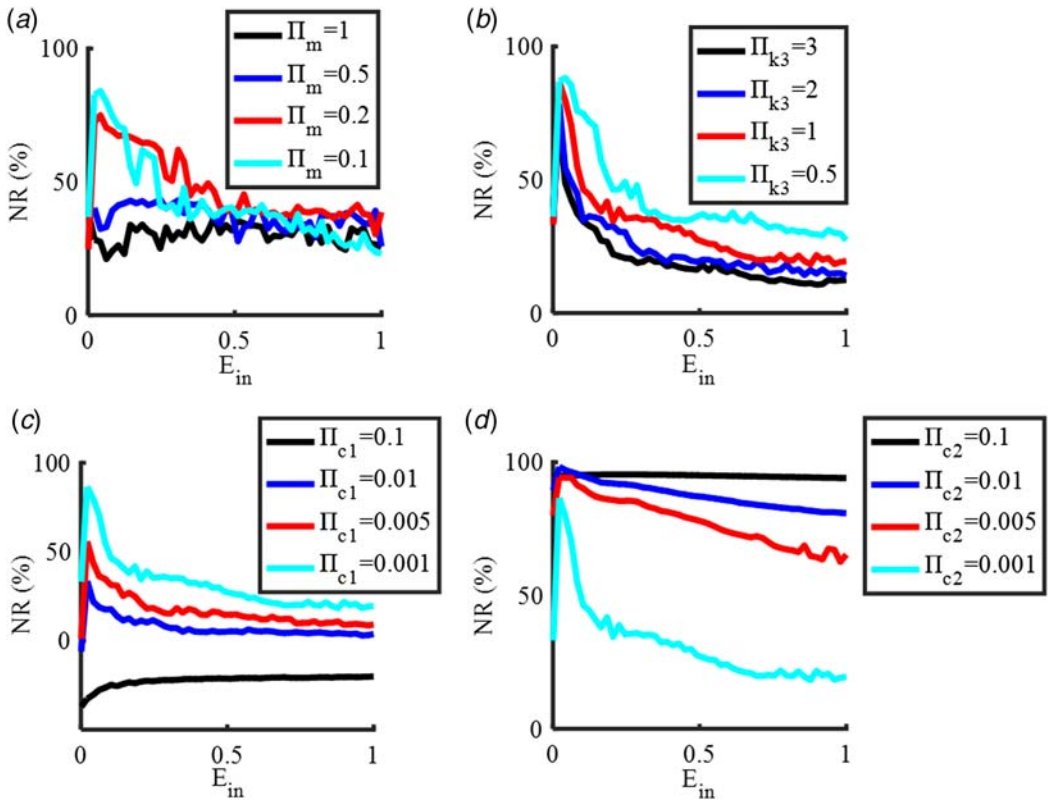

Fig. 6 Effect of varying dimensionless parameters on local nonreciprocity: varying Π_m (*a*), Π_{k_3}(*b*), Π_{c_1} (*c*), and Π_{c_2}(*d*). When not varied, $\Pi_m = 0.05$ (*b,c,d*), $\Pi_{k_3} = 1$ (*a,c,d*), $\Pi_{c_1} = 0.001$ (*a,b,d*), and $\Pi_{c_2} = 0.001$ (*a,b,c*).

at the large scale (such that $|q_1| \sim 1$ and $|q_2| \ll 1$ for $\Pi_m \ll 1$). Initial velocities correspond to a constant dimensionless energy, E_{in}, applied to either scale

$$Q_0' = \begin{cases} \sqrt{2E_{in}} & \text{(LS excitation)} \\ \sqrt{\dfrac{2E_{in}}{\Pi_m}} & \text{(SS excitation)} \end{cases} \tag{11}$$

These nondimensionalized equations can be numerically integrated to determine the relationship between the relative sizes of the unit cell parameters and the local nonreciprocity. The degree of nonreciprocity (NR), is a dimensionless measure of local nonreciprocity in the two-scale system is

$$NR = \frac{E_{D,1} - E_{D,2}}{E_{in}} \tag{12}$$

where

$$E_{D,1} = \lim_{T\to\infty} \frac{\int_0^T \Pi_{c_2}(q_1' - q_2')^2 d\tau}{E_{in}} \tag{13}$$

$$E_{D,2} = \lim_{T\to\infty} \frac{\int_0^T \Pi_{c_1}(q_1')^2 d\tau}{E_{in}} \tag{14}$$

and $E_{D,1}$ and $E_{D,2}$ are computed for LS and SS excitations, respectively.

Results of measuring NR in Eq. (12) while varying the four dimensionless parameters are presented in Fig. 6. It is apparent that *large mass ratios* and *low-stiffness nonlinearities* are significant for inducing nonreciprocity. While the study on varying Π_{c_2} suggests that large values of damping between the two scales (i.e., large c_2 values) is desirable to design for nonreciprocity, such systems rapidly reduce the system's available kinetic energy and therefore are likely not useful in the lattice configuration where energy propagation over long distances may be desired. Similarly, negative values of NR for $\Pi_{c1} = 0.1$ demonstrate that, for sufficiently large values of the grounding damper, energy prefers to dissipate at the LS regardless of the scale that is excited.

4 Global Nonreciprocity Study

The global periodic configuration of the hierarchical structure is now considered for both narrowband and broadband excitation. Considering now the three-scale system depicted in Fig. 2, the jth unit cell is governed by

$$m_{outer}\ddot{x}_{outer}(j) + c_{outer}\dot{x}_{outer}(j) + c_{middle}(\dot{x}_{outer}(j) - \dot{x}_{middle}(j)) + k_1(2x_{outer}(j) - x_{inner}(j-1)) + k_{3,middle}(x_{outer}(j) - x_{middle}(j))^3 = 0 \tag{15}$$

$$m_{middle}\ddot{x}_{middle}(j) + c_{middle}(\dot{x}_{middle}(j) - \dot{x}_{outer}(j)) + c_{inner}(\dot{x}_{middle}(j) - \dot{x}_{inner}(j)) + k_{3,middle}(x_{middle}(j) - x_{outer}(j))^3 + k_{3,inner}(x_{middle}(j) - x_{inner}(j))^3 = 0 \tag{16}$$

$$m_{inner}\ddot{x}_{inner}(j) + c_{inner}(\dot{x}_{inner}(j) - \dot{x}_{middle}(j)) + k_1(x_{inner}(j) - x_{outer}(j+1)) + k_{3,inner}(x_{inner}(j) - x_{middle}(j))^3 = 0 \tag{17}$$

Informed by the 1:1 TRC that governs the nonreciprocity in an isolated unit cell [21], results from direct numerical simulation of the lattice equations of motion strongly suggest that TRC governs the global breaking of reciprocity for wave propagation in the lattice structure. The study considers both broadband (impulsive) and narrowband (harmonic) external excitations. Systems with both two and three scales will be discussed to demonstrate the generality of the hierarchical structure design and the effect of nesting varying number of scales will be presented for impulsive excitation.

4.1 Broadband Excitation. The first part of the study concerns broadband (impulsive) excitations applied either at the free boundaries or at the middle of the nonlinear lattice. When assigning impulses to the 1D chain, it is convenient to express their magnitude relative to I_{norm}, the maximum momentum associated with a plane wave in a linear monoatomic chain

$$I_{norm} = m_{outer} v_{g,max} \tag{18}$$

where $v_{g,max}$ is the maximum group velocity of the monoatomic chain [26] formed by m_{outer} and coupling and grounding springs of stiffness k_1:

$$v_{g,max} = \max\left(\frac{k_1 \sin\mu}{m_{outer}\omega_0}\right) \tag{19}$$

where $\omega_0 = \sqrt{(k_1/m)(3 - 2\cos\mu)}$ and μ is the dimensionless wavenumber/propagation constant. Figure 7 presents results for impulsively exciting the largest mass of the three scale unit cell with $I_0 = 7.36\, I_{norm}$ at the center of a chain composed of 50 unit cells. Lattices are terminated with the convention depicted in Fig. 3, in which the

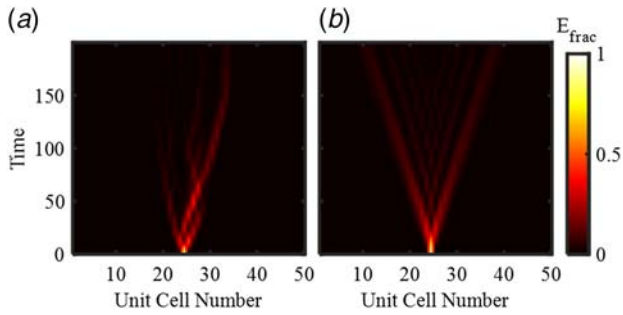

Fig. 7 Impulsive excitation of the large scale of the unit cell at the chain's center in a nonlinear (*a*) and linear (*b*) lattice. Note the preferential propagation of energy from left-to-right for the case with nonlinear interactions: $m_{outer} = 1$, $m_{middle} = 0.05$, $m_{inner} = 0.005$, $k_1 = 1$, $k_{1,middle} = 0$, $k_{1,inner} = 0$, $k_{3,middle} = 1$, $k_{3,inner} = 0.1$, $c_{outer} = 0.002$, $c_{middle} = 0.002$, $c_{inner} = 0.0002$, $I_0/I_{norm} = 7.36$. For (*b*), $k_{3,middle}$ and $k_{3,inner}$ govern linear restoring forces.

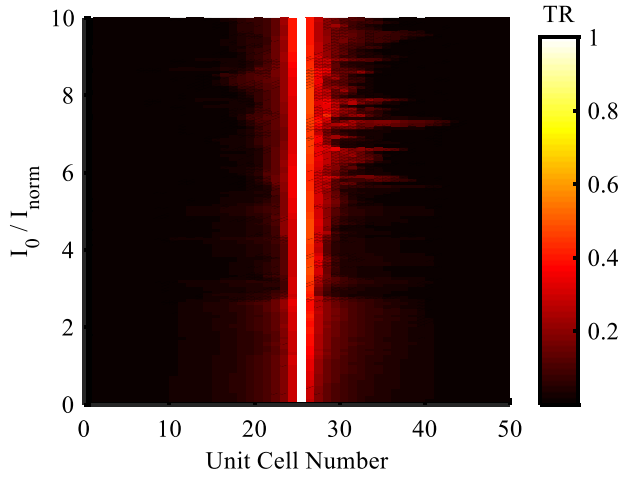

Fig. 8 Response of a 1D lattice to various impulse amplitudes applied to the large scale of the unit cell at its center. Nonreciprocal behavior occurs at specific impulse magnitudes: $m_{outer} = 1$, $m_{middle} = 0.05$, $m_{inner} = 0.005$, $k_1 = 1$, $k_{1,middle} = 0.05$, $k_{1,inner} = 0.05$, $k_{3,middle} = 1$, $k_{3,inner} = 0.1$, $c_{outer} = 0.002$, $c_{middle} = 0.002$, $c_{inner} = 0.0002$.

first and last unit cells are linearly grounded. As with the local study of the previous section, nonzero initial velocity V_0 applied to a single unit cell of the system model impulses. In all cases considered, the impulses are applied to the corresponding large scales of the unit cells. The quantity E_{frac} is the fraction of energy at the unit cell relative to the energy delivered to the system by the impulse, $(1/2)m_{outer}V_0^2$. As a reference, essentially nonlinear springs are replaced by linear springs with the same spring constants in Fig. 7(*b*). For the nonlinear case, note the considerably different behavior of energy propagation to the left of the center as compared with the right: *energy preferentially travels from left-to-right, thus indicating a global breaking of acoustic reciprocity*. Energy radiates symmetrically outward in Fig. 7(*b*) highlighting the crucial role that nonlinearity plays for breaking reciprocity in this lattice structure.

To quantify the amount of transmission in the lattice, a transmission ratio *TR* is defined to be

$$TR = \frac{\max(PE + KE)}{\frac{1}{2}m_{outer}V_0^2} \tag{20}$$

where $\max(PE+KE)$ is the maximum sum of potential and kinetic energy that occurs for each unit cell across all time in a simulation.

Figure 8 depicts the results of applying various impulse values to the large scale of the unit cell at the center of a chain with 50 unit cells, with *TR* computed at each impulse value. Note that nonreciprocity activates when $6 < I_0/I_{norm} < 8$, as indicated by the preference for left-to-right over right-to-left propagation. The highest degree of nonreciprocity occurs near $I_0/I_{norm} = 7.5$; however, this effect weakens for larger impulse amplitudes as the response becomes more symmetrical. Such a result is reminiscent of the response of the two-scale isolated unit cell in Fig. 5 in which TRC takes effect when the impulse magnitude falls within a well-defined range of values for breaking reciprocity.

Figure 9 presents the results of applying an impulse of $I_0 = 0.1$ I_{norm} to the large scale at the left and right boundaries of the chain (in separate simulations). These results again demonstrate that energy propagates from left-to-right but not right-to-left. Note that weak linear springs of stiffness $k_{1,middle}$, $k_{1,inner}$ are added in parallel to the nonlinear stiffnesses $k_{3,middle}$, $k_{3,inner}$, respectively, to increase the wave's range, though they are not necessary for inducing nonreciprocity. The minimal effect of weak linear terms in parallel with strongly nonlinear forces on the global nonreciprocity in this lattice was experimentally confirmed in Ref. [22].

Figure 10 displays results from exciting the large scales of the unit cells at the chain's left and right boundaries with various impulse values. As with the center excitation, nonreciprocity occurs at a finite range of impulse amplitudes. It is important to note that the preferential transmission of energy from left-to-right and not right-to-left is unaffected by the direction of the impulse delivered

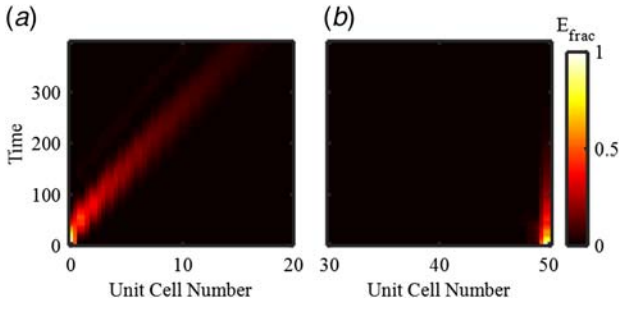

Fig. 9 Impulsive excitation of the large scale of the unit cells at the chain's boundaries. Energy propagates rightward when initiated at the left boundary (*a*) but localizes when initiated at the right boundary (*b*): $m_{outer} = 1$, $m_{middle} = 0.05$, $m_{inner} = 0.005$, $k_1 = 1$, $k_{1,middle} = 0.05$, $k_{1,inner} = 0.05$, $k_{3,middle} = 1$, $k_{3,inner} = 0.1$, $c_{outer} = 0.002$, $c_{middle} = 0.002$, $c_{inner} = 0.0002$, $I_0/I_{norm} = 0.1$.

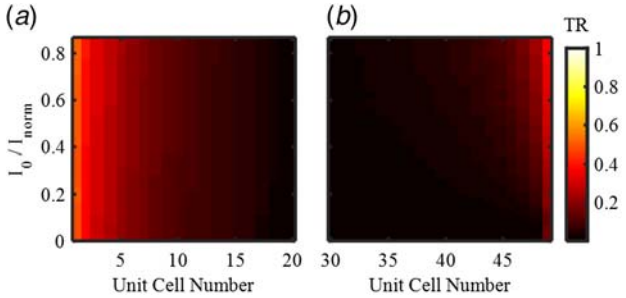

Fig. 10 Response of a 1D lattice to various impulse amplitudes applied to the large scale of the unit cells at the left (*a*) and right (*b*) boundaries. The preferential energy propagation occurs at various impulse amplitudes: $m_{outer} = 1$, $m_{middle} = 0.05$, $m_{inner} = 0.005$, $k_1 = 1$, $k_{1,middle} = 0.05$, $k_{1,inner} = 0.05$, $k_{3,middle} = 1$, $k_{3,inner} = 0.1$, $c_{outer} = 0.002$, $c_{middle} = 0.002$, $c_{inner} = 0.0002$.

to the outer mass, i.e., leftward directed initial momentum ($I_0 < 0$) produces nearly identical results. It is also interesting to note that exciting the chain's boundaries requires smaller impulse magnitudes to break reciprocity as compared with exciting the chain's center.

Unlike systems with an interface [16–18], defects [19], or an isolated unit cell [21], the lattice studied herein will induce asymmetric wave propagation at any location—even at its boundaries. Further analytical investigation of the lattice equations of motion will also be considered in future work.

As further numerical evidence of acoustic nonreciprocity in the nonlinear lattice considered, Figs. 11 and 12 depict the results of numerical simulations of a lattice composed of 21 unit cells, possessing the internal hierarchy, asymmetry, and nonlinear features discussed previously. Contrary to the results in Figs. 7 through 10, which correspond to a hierarchy of three internal scales in each cell, in the following results each unit cell contains just two scales (that is, a large-scale nonlinearly coupled to a small scale) with system parameters as follows: $m_{outer} = 1.0$, $m_{inner} = 0.05$, $k_1 = 1.0$, $k_{3,inner} = 1.0$, $c_{outer} = c_{inner} = 0.002$.

Figure 11 presents the instantaneous energies of the unit cells of the nonlinear lattice for a relatively low-intensity impulse $I_0/I_{norm} = 0.57$ applied to the large scale of the left (*a*,*d*), middle (*b*,*e*), and right (*c*,*f*) unit cell of the lattice. Each case depicts the spatiotemporal evolution of the instantaneous energies of the cells, together with the transient variations of selected unit cells. The instantaneous energies are normalized with respect to the kinetic energy delivered to the lattice by the impulse. Note the presence of rightward wave propagation for left boundary impulsive excitation (Fig. 11(*d*)) and absence of leftward wave propagation for right boundary impulsive excitation (Fig. 11(*f*)); in the latter case, also note the response localization at the right boundary of the lattice. Although some degree of nonreciprocity is noted for impulsive excitation of the middle cell of the lattice (Fig. 11(*e*)), it is weak, with preferential leftward wave propagation.

Figure 12 depicts the corresponding unit cell energy variations for the case of higher impulse intensity $I_0/I_{norm} = 0.79$. Although acoustic nonreciprocity still exists in the lattice, in this case, there is both rightward and leftward wave transmission indicating that a bifurcation has occurred and the mode of acoustic nonreciprocity has now changed. It is important to note that this bifurcation was qualitatively observed in experiments in Ref. [22]. The theoretical analysis of such bifurcations in the nonlinear acoustics of the considered lattice will be examined in future work.

The following explanation proposes the sequence of events that determine the global breaking of acoustic reciprocity in the lattice with nonlinearity, asymmetry, and internal scale hierarchy excited at its boundaries:

Left-to-right: The directly excited large scale of the leftmost unit cell oscillates at a predefined natural frequency due to the

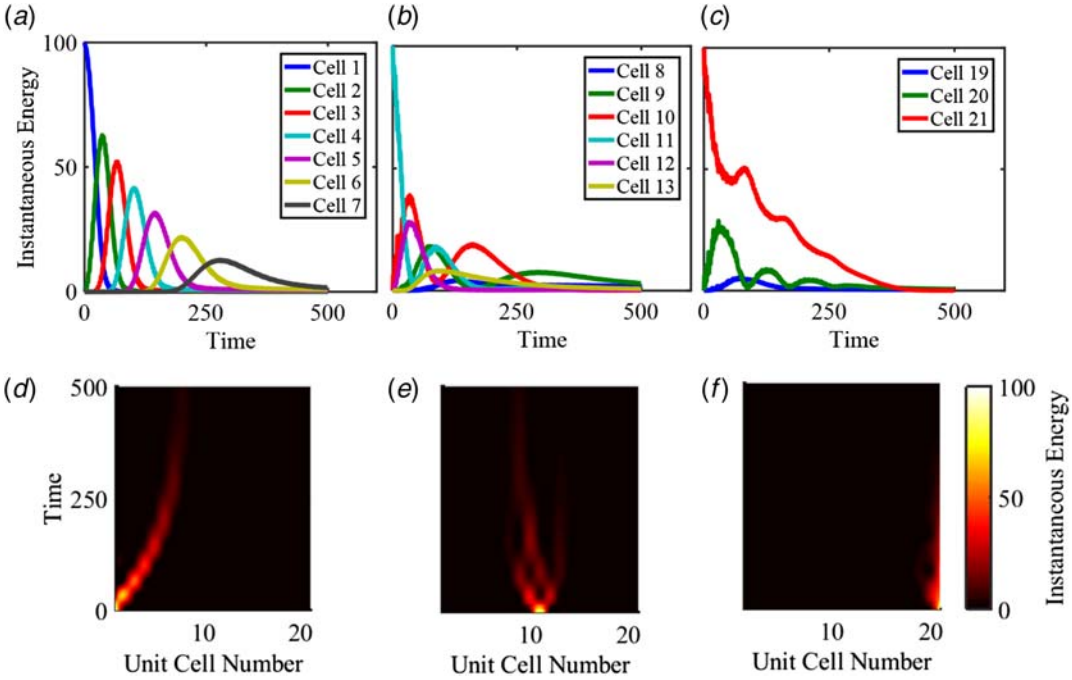

Fig. 11 Acoustics of the 21-unit cell nonlinear lattice for relatively low-intensity excitation of the large scale of the left cell (*a,d*), middle cell (*b,e*), and right cell (*c,f*). Upper plots (*a,b,c*) depict the variations of the instantaneous energies of selected unit cells and lower plots (*d,e,f*) the spatiotemporal variations of the instantaneous cell energies of the lattice: $m_{outer} = 1.0$, $m_{inner} = 0.05$, $k_1 = 1.0$, $k_{3,inner} = 1.0$, $c_{outer} = 0.002$, $c_{inner} = 0.002$.

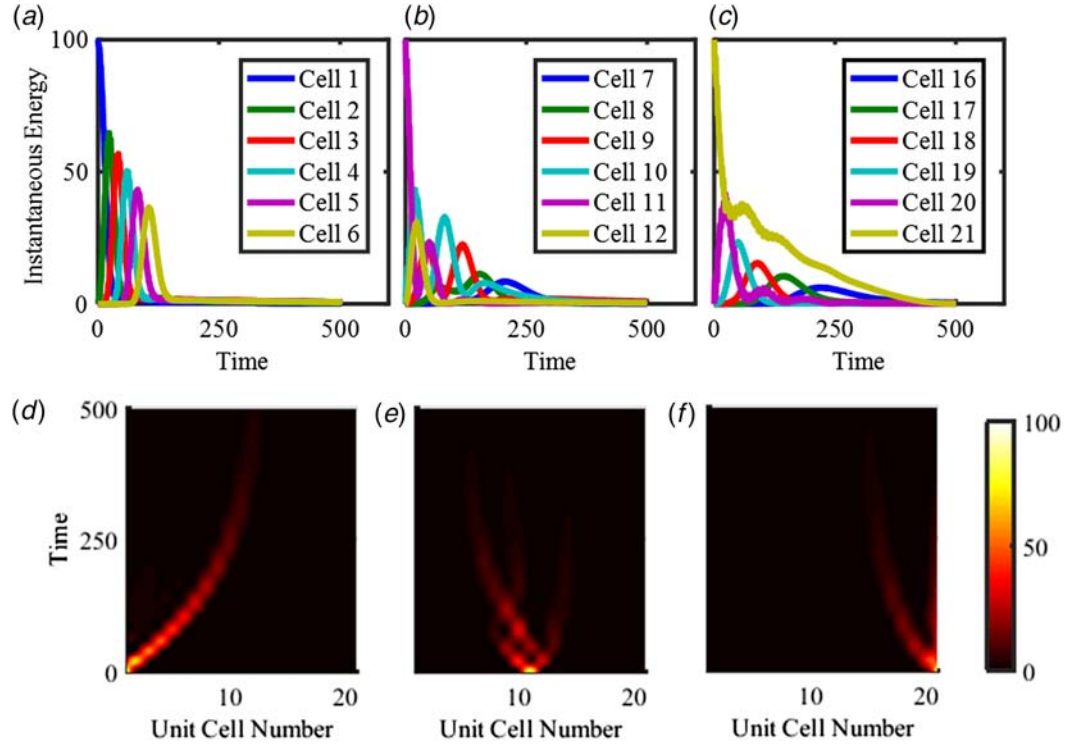

Fig. 12 Acoustics of the 21-unit cell nonlinear lattice for higher-intensity excitation of the large scale of the left cell (*a,d*), middle cell (*b,e*), and right cell (*c,f*). Upper plots (*a,b,c*) depict the variations of the instantaneous energies of selected unit cells and lower plots (*d,e,f*) the spatiotemporal variations of the instantaneous cell energies of the lattice: $m_{outer} = 1.0$, $m_{inner} = 0.05$, $k_1 = 1.0$, $k_{3,inner} = 1.0$, $c_{outer} = c_{inner} = 0.002$.

linear grounding spring. Assuming enough energy is in the system from the impulse, energy transfers from the large scale to the next smallest scale via 1:1 transient resonance capture [21] associated with the cubically nonlinear spring, and it continues to transmit down to each successively smaller scale. When the energy arrives at the smallest scale, it can then readily flow to the largest scale of its neighboring unit cell on the right because of the linear coupling spring. The process then repeats and a wave propagates from left-to-right.

Right-to-left: Energy transfers from the directly excited large scale of the rightmost unit cell to the smallest scale of its neighboring unit cell on the left because of the linear coupling spring. However, energy cannot transmit from the small scale to the large scale and is ultimately dissipated at the smallest scale due to the failure to initiate TRC, as evidenced by the results in the local study. Thus, energy is arrested and waves cannot propagate from right-to-left.

This design scheme could be added to systems to redirect mechanical shock and vibration. For example, adding this lattice to buildings, bridges, or aircraft could achieve a variety of purposes: to protect diagnostic sensors from being contaminated by unwanted mechanical disturbances, to focus energy toward structural health monitoring equipment, or to direct energy away from sensitive structural components.

In the local study in Sec. 3, damping plays an important role in trapping energy at the small scale (see Fig. 5). Consequently, it was considered in the lattice and, while it limited the wave's range, demonstrated that highly asymmetric wave propagation can be achieved in dissipative media. Since the proposed lattice would be fabricated and added to systems, the degree of damping is largely in control of the design engineer. Careful unit cell design can increase or decrease damping as desired.

The effect of nesting different numbers of small scales within each unit cell for impulses applied to the center of the lattice is displayed in Fig. 13. The amount of global nonreciprocity in each simulation, NR_G, is computed as

$$NR_G = \frac{\max(E_R) - \max(E_L)}{\frac{1}{2} m_{outer} V_0^2} \tag{21}$$

where E_R and E_L denote the maximum amounts of energy transmitted to the left and right sides of the impulse, respectively, and V_0 denotes the outer mass' initial velocity due to the impulse. Note that the threshold impulse value for nonreciprocity increases as the number of nested masses, M, increases.

While Fig. 13 indicates that nesting $M = 5$ masses is most desirable to break reciprocity across a large range of impulse amplitudes, practical implementation of such a design likely is technically challenging. Particularly, fabrication of a structure with mass and linear/nonlinear stiffness values that span five orders of magnitude would likely pose challenges for assembly, weight, structural integrity, and cost. Current work focuses on this particular fabrication aspect as well.

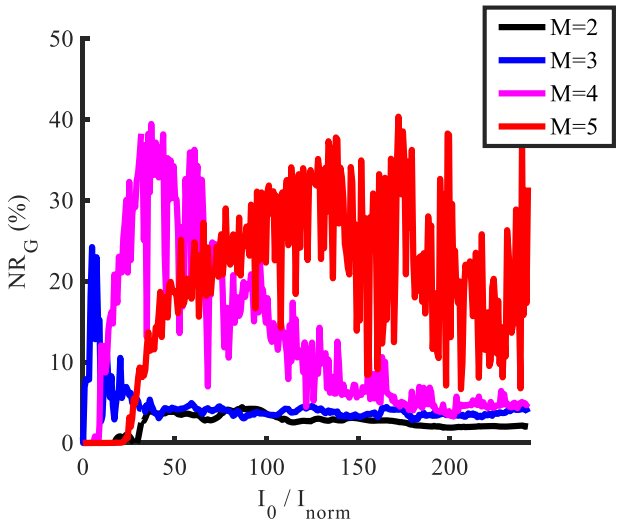

Fig. 13 Effect of nesting different numbers of small scales in each unit cell on global nonreciprocity. An increased number of nested masses enhances the nonreciprocal behavior over a range of impulse amplitudes

4.1.1 Internal Resonator Design. A variant of the hierarchical structure design of the lattice with three-scale internal hierarchy is to couple the intermediate small scale (i.e., the middle mass) instead of the smallest scale (i.e., the innermost mass) to the neighboring unit cell's large scale, thus creating an *internal resonator* with the small scale, as pictured in Fig. 14. Such configuration is reminiscent of other systems using internal resonators to attenuate energy flow of waves in periodic structures [27,28].

Its corresponding equations of motion for the jth unit cell is

$$m_{outer}\ddot{x}_{outer}(j) + c_{outer}\dot{x}_{outer}(j) + c_{middle}(\dot{x}_{outer}(j) - \dot{x}_{middle}(j)) + k_1(2x_{outer}(j) - x_{middle}(j-1)) + k_{3,middle}(x_{outer}(j) - x_{middle}(j))^3 = 0 \tag{22}$$

$$m_{middle}\ddot{x}_{middle}(j) + c_{middle}(\dot{x}_{middle}(j) - \dot{x}_{outer}(j)) + c_{inner}(\dot{x}_{middle}(j) - \dot{x}_{inner}(j)) + k_1(x_{middle}(j) - x_{outer}(j+1)) + k_{3,middle}(x_{middle}(j) - x_{outer}(j))^3 + k_{3,inner}(x_{middle}(j) - x_{inner}(j))^3 = 0 \tag{23}$$

$$m_{inner}\ddot{x}_{inner}(j) + c_{inner}(\dot{x}_{inner}(j) - \dot{x}_{middle}(j)) + k_{3,inner}(x_{inner}(j) - x_{middle}(j))^3 = 0 \tag{24}$$

Figure 15 presents the results from applying various impulse amplitudes to this alternative lattice design. Note that nonreciprocity occurs in this system as well, but it takes larger impulse values to initiate as compared to the system design considered previously. Also note that the nonreciprocity begins to weaken as impulse amplitude approaches values near $I_0 = I_{norm}$, which further supports that TRC occurs in the lattice structure.

4.2 Narrowband Excitation. The second aspect of this computational study is concerned with narrowband excitations, in the form of harmonic applied loads. Again, excitation of the large scale of a specific unit cell is considered. As with broadband excitation, energy transmission is measured. The forcing is

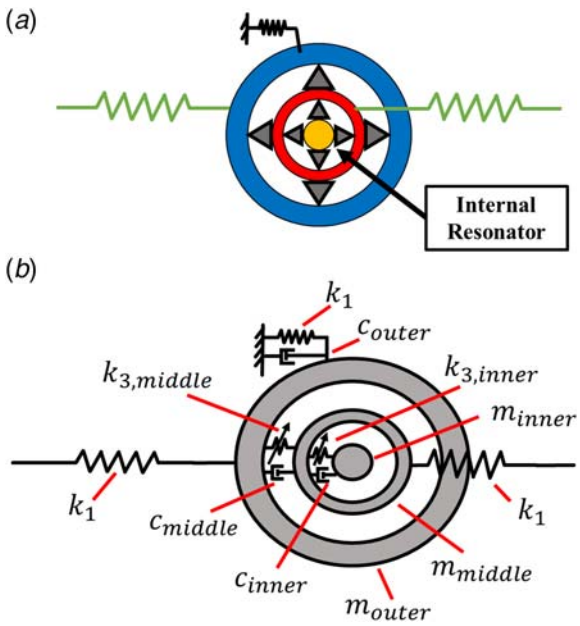

Fig. 14 Internal resonator design: (*a*) elastomeric bumper fabrication strategy and (*b*) equivalent spring-mass-damper representation

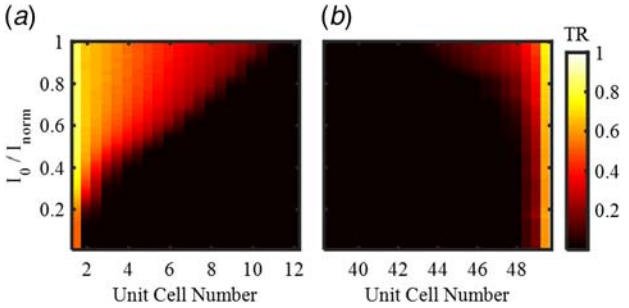

Fig. 15 Response to various impulse amplitudes on the left (*a*) and right (*b*) boundaries of the internal resonator design. Nonreciprocity occurs over a finite range of amplitudes. $m_{outer} = 1$, $m_{middle} = 0.05$, $m_{inner} = 0.005$, $k_1 = 1$, $k_{3,middle} = 1$, $k_{3,inner} = 0.1$, $c_{outer} = 0.002$, $c_{middle} = 0.002$, $c_{inner} = 0.0002$.

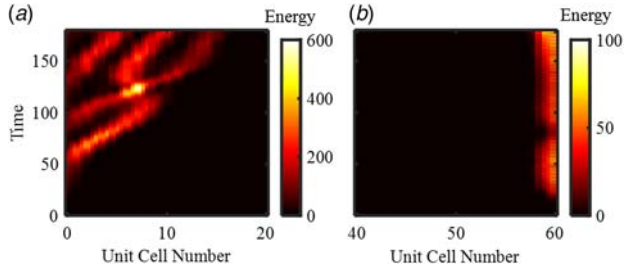

Fig. 17 Harmonic excitation of the lattice at the large scale of the unit cell on the left (*a*) and right (*b*) boundaries of the lattice. Propagating waves are generated from forcing at the left boundary while evanescent waves are generated from forcing at the right boundary: $m_{outer} = 1$, $m_{middle} = 0.05$, $m_{inner} = 0.005$, $k_1 = 1$, $k_{1,middle} = 0.05$, $k_{1,inner} = 0.05$, $k_{3,middle} = 1$, $k_{3,inner} = 0.1$, $c_{outer} = 0.002$, $c_{middle} = 0.002$, $c_{inner} = 0.0002$, $F_0 = 6.67$, $\omega = 1.6$.

parameterized by both an amplitude F_0 and frequency ω, i.e., $F(t) = F_0 \sin \omega t$ applied to the large scale at either the boundaries of the lattice or at its center.

A case study with a 60-cell lattice exhibiting this nonreciprocal behavior is pictured in Fig. 16 with a forcing of amplitude $F_0 = 4.37$ and frequency $\omega = 1.6$ applied to the outer mass. The first and last unit cells are grounded as presented in Fig. 3. As with impulses applied to the lattice's center, asymmetrical wave propagation develops indicating a global breaking of reciprocity.

Figure 17 displays the results from exciting the large scale at the left or right boundaries of the lattice with $F_0 = 6.67$ and frequency $\omega = 1.6$. Note that again, left-to-right transmission occurs but not right-to-left.

To characterize the relationship between frequency and propagation, a dispersion analysis of wave propagation in the three-scale lattice is conducted. It is desired to compute a wavenumber μ (or, more accurately, a propagation constant with units [radians/unit cell index]) for a given forcing frequency ω. A linear spring of variable stiffness $k_{1,d}$ is added in parallel with both $k_{3,middle}$ and $k_{3,inner}$. Various lattices are tested in which values of $k_{1,d}$ are decreased from a large value to a small value, thus starting at a nearly linear lattice (with therefore a well-defined dispersion curve) and arriving at one that is strongly nonlinear.

The real part of μ at each forcing frequency is computed by taking the phase differences between the complex amplitude of two adjacent outer masses' displacement fast Fourier transform (FFTs) taken over time and evaluated at the forcing frequency [29]. If the temporal FFT of the outer mass at the nth unit cell transforms displacements into the frequency domain ($x(n, t) \rightarrow Z(n, \Omega)$), then the real component of the propagation constant is

$$\mathrm{Re}(\mu(\omega)) = \frac{\arg(Z(n_2, \omega)) - \arg(Z(n_1, \omega))}{n_2 - n_1} \tag{25}$$

where n_1 and n_2 are arbitrary unit cells numbered in increasing order from left to right and Ω is set to the forcing frequency ω.

The imaginary part of μ is found by examining spatial amplitude decay of the near-field (local wave) when it exists. For a given forcing frequency ω, if the peak displacement of the outer mass at the nth unit cell is $X(n, \omega)$, then the imaginary component of the propagation constant is

$$\mathrm{Im}(\mu(\omega)) = \frac{1}{n_2 - n_1} \ln\left(\frac{X(n_1, \omega)}{X(n_2, \omega)}\right) \tag{26}$$

By the sign convention in Eqs. (25) and (26), $\mu > 0$ denotes rightward propagation (from forcing at the left boundary) and $\mu < 0$ denotes leftward propagation (from forcing at the right boundary). Figure 18 presents the results of this dispersion analysis. Note that nonreciprocity begins to take effect at the *band edge* (cutoff frequency or final coordinate of the irreducible Brillouin zone [26]) when $k_{1,d}$ is sufficiently small, suggesting that energy must be built-up to activate transient resonance capture. High-energy activation of nonreciprocal behavior parallels the amplitude-dependent TRC that is known to occur in the isolated unit cell. The near zero group velocity, $d\omega/d\mu$, intrinsic to the band edge makes this energy build-up feasible. Note the disparity in the computed wavenumber for leftward ($\mu < 0$) and rightward ($\mu > 0$) waves for the lattices with smaller values of $k_{1,d}$. For $k_{1,d} = 0.1$ and 1, $\mathrm{Re}(\mu(\omega))$ goes to π for leftward propagation (indicating an evanescent wave) but not for rightward propagation (indicating a propagating wave).

By observation of Figs. 16 and 17, it is apparent that the real component of μ is rather complicated for nonreciprocal parameter sets: group velocity varies over space and waves reflect backward creating exotic interference patterns. Consequently, the real component of μ at the band edge in Fig. 18 is not intended to be a single representative value for the propagation constant at the given forcing frequency, but rather an average value taken over a series of unit cells.

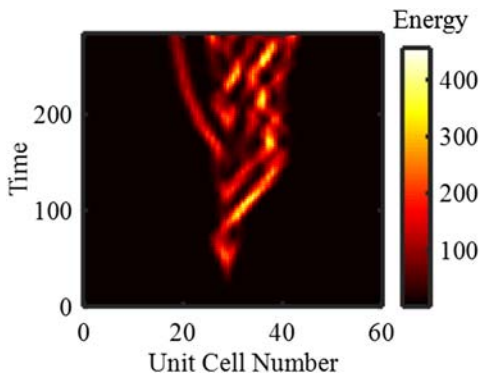

Fig. 16 Harmonic excitation of the lattice at the large scale of the unit cell in its center. Energy primarily distributes at the right side of the forcing: $m_{outer} = 1$, $m_{middle} = 0.05$, $m_{inner} = 0.005$, $k_1 = 1$, $k_{1,middle} = 0.05$, $k_{1,inner} = 0.05$, $k_{3,middle} = 1$, $k_{3,inner} = 0.1$, $c_{outer} = 0.002$, $c_{middle} = 0.002$, $c_{inner} = 0.0002$, $F_0 = 4.37$, $\omega = 1.6$.

5 Concluding Remarks

Nonlinear acoustic nonreciprocity is reported for a lattice structure exhibiting asymmetry and purely cubic stiffness nonlinearity in its unit cell design. Studying the dynamics of an isolated unit cell reveals that transient resonance capture governs the breaking of reciprocity when the system energy lies within a critical range of values. Direct numerical simulation of the lattice's equations of motion when subjected to both broadband and narrowband excitation yields asymmetrical wave propagation. The global

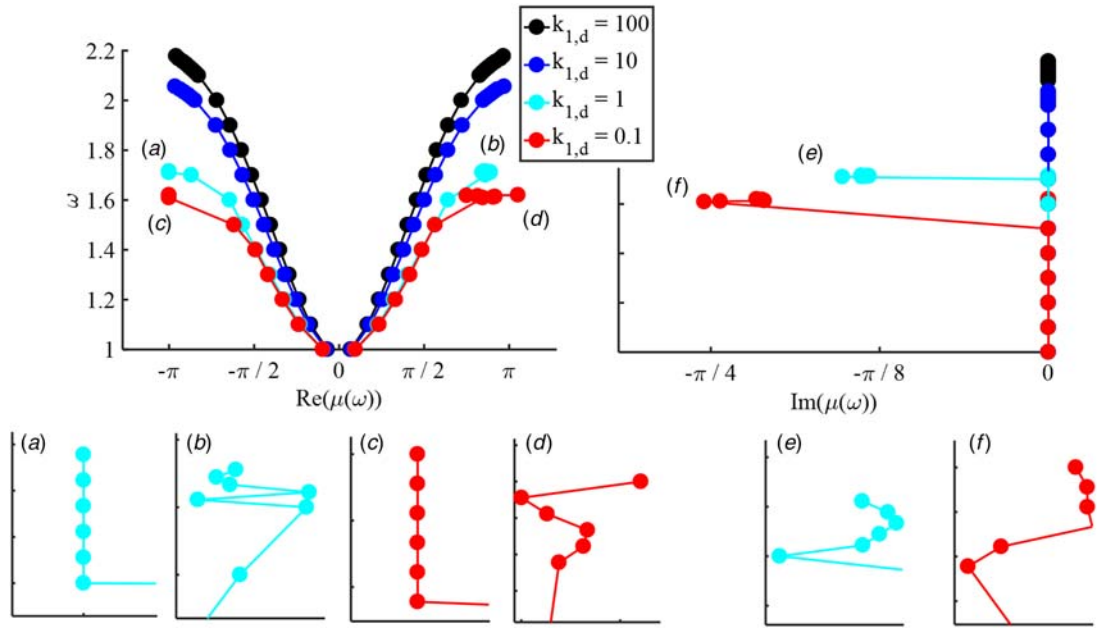

Fig. 18 Dispersion analysis for three degree-of-freedom lattice structure. Nonreciprocal propagation occurs at the band edge when the coupling between nested masses is predominantly nonlinear. Asymmetrical propagation is evident by comparing the real part of the wavenumber for each forcing frequency (*a,b,c,d*) to the imaginary part (*e,f*) of the wavenumber for leftward and rightward waves. $m_{outer} = 1$, $m_{middle} = 0.05$, $m_{inner} = 0.005$, $k_1 = 1$, $k_{1,middle} = 0.05$, $k_{1,inner} = 0.05$, $k_{3,middle} = 1$, $k_{3,inner} = 0.1$, $c_{outer} = 0.002$, $c_{middle} = 0.002$, $c_{inner} = 0.0002$, $F_0 = 6.67$.

nonreciprocity activates at higher energy levels, providing strong evidence that transient resonance capture induces this behavior. Because this is a passive structure, these findings could be useful for shock and noise mitigation applications.

Acknowledgment

This research was supported in part by the National Science Foundation (Emerging Frontiers Research Initiative NewLAW Program) through Grants 1332862 and 1741565. Shuangbao Li is grateful for the support of the National Natural Science Foundation of China (NNSFC) through Grant No. 11472298; Funder ID: 10.13039/501100001809 which made possible his visiting appointment at the University of Illinois at Urbana–Champaign.

Funding Data

- Directorate for Engineering and International Cooperation and Exchange Programme.

References

[1] Courant, R., and Hilbert, D., 1989, *Methods of Mathematical Physics*, Wiley-VCH, Weinheim, Germany.
[2] Casimir, H. B. G., 1945, "On Onsager's Principle of Microscopic Reversibility," Rev. Mod. Phys., **17**(2–3), pp. 343–350.
[3] Onsager, L., 1931, "Reciprocal Relations in Irreversible Processes. I," Phys. Rev., **37**(4), pp. 405–426.
[4] Onsager, L., 1931, "Reciprocal Relations in Irreversible Processes. II," Phys. Rev., **38**(12), pp. 2265–2279.
[5] Fleury, R., Sounas, D., Haberman, M. R., and Alu, A., 2015, "Nonreciprocal Acoustics," Acoust. Today, **11**, pp. 14–21.
[6] Arntzenius, F., and Greaves, H., 2009, "Time Reversal in Classical Electromagnetism," Br. J. Philos. Sci., **60**(3), pp. 557–584.
[7] Kittel, C., 1958, "Interaction of Spin Waves and Ultrasonic Waves in Ferromagnetic Crystals," Phys. Rev., **110**(4), pp. 836–841.
[8] Fleury, R., Sounas, D. L., Sieck, C. F., Haberman, M. R., and Alu, A., 2014, "Sound Isolation and Giant Linear Nonreciprocity in a Compact Acoustic Circulator," Science, **343**(6170), pp. 516–519.
[9] Quan, L., Sounas, D., and Alu, A., 2017, "Non-reciprocal Sound Propagation in Zero-Index Metamaterials," J. Acoust. Soc. Am., **141**(5), pp. 3698–3698.
[10] Trainiti, G., and Ruzzene, M., 2016, "Non-Reciprocal Elastic Wave Propagation in Spatiotemporal Periodic Structures," New J. Phys., **18**(8), p. 083047.
[11] Nassar, H., Xu, X. C., Norris, A. N., and Huang, G. L., 2017, "Modulated Phononic Crystals: Non-Reciprocal Wave Propagation and Willis Materials," J. Mech. Phys. Solids, **101**, pp. 10–29.
[12] Attarzadeh, M. A., and Nouh, M., 2018, "Non-Reciprocal Elastic Wave Propagation in 2D Phononic Membranes With Spatiotemporally Varying Material Properties," J. Sound Vib. **422**, pp. 264–277.
[13] Seif, A., DeGottardi, W., Esfarjani, K., and Hafezi, M., 2018, "Thermal Management and Non-Reciprocal Control of Phonon Flow via Optomechanics," Nat. Commun., **9**(1), p. 1207.
[14] Croënne, C., Vasseur, J. O., Matar, O. B., Ponge, M.-F., Deymeir, P. A., Hladky-Hennion, A.-C., and Dubus, B., 2017, "Brillouin Scattering-Like Effect and Non-Reciprocal Propagation of Elastic Waves due to Spatio-Temporal Modulation of Electrical Boundary Conditions in Piezoelectric Media," Appl. Phys. Lett., **110**(6), p. 061901.
[15] Ansari, M. H., Attarzadeh, M. A., Nouh, M., and Karami, M. A., 2018, "Application of Magnetoelastic Materials in Spatiotemporally Modulated Phononic Crystals for Nonreciprocal Wave Propagation," Smart Mater. Struct., **27**(1), p. 015030.
[16] Liang, B., Guo, X. S., Tu, J., Zhang, D., and Cheng, J. C., 2010, "An Acoustic Rectifier," Nat. Mater., **9**(12), pp. 989–992.
[17] Liang, B., Yuan, B., and Cheng, J.-C., 2009, "Acoustic Diode: Rectification of Acoustic Energy Flux in One-Dimensional Systems," Phys. Rev. Lett., **103**(10), p. 104301.
[18] Luo, B., Gao, S., Liu, J., Mao, Y., Li, Y., and Liu, X., 2018, "Non-Reciprocal Wave Propagation in One-Dimensional Nonlinear Periodic Structures," AIP Adv., **8**(1), p. 015113.
[19] Boechler, N., Theocharis, G., and Daraio, C., 2011, "Bifurcation-Based Acoustic Switching and Rectification," Nat. Mater., **10**(9), pp. 665–668.
[20] Wu, Z., and Wang, K. W., 2017, "A Metastable Modular Structural System for Adaptive Nonreciprocal Wave Propagation," Proceedings of the SPIE Smart Structures and Materials + Nondestructive Evaluation and Health Monitoring, Portland, OR, Apr. 11, 2017, p. 1016412.
[21] Moore, K. J., Bunyan, J., Tawfick, S., Gendelman, O. V., Li, S., Leamy, M., and Vakakis, A. F., 2018, "Nonreciprocity in the Dynamics of Coupled Oscillators With Nonlinearity, Asymmetry, and Scale Hierarchy," Phys. Rev. E, **97**(1), p. 012219.
[22] Bunyan, J., Moore, K. J., Mojahed, A., Fronk, M. D., Leamy, M., Tawfick, S., and Vakakis, A. F., 2018, "Acoustic Nonreciprocity in a Lattice Incorporating Nonlinearity, Asymmetry, and Internal Scale Hierarchy: Experimental Study," Phys. Rev. E, **97**(5), p. 052211.
[23] Luo, J., Wierschem, N. E., Fahnestock, L. A., Bergman, L. A., Spencer, B. F., Jr., Al-Shudeifat, M., McFarland, D. M., Quinn, D. D., and Vakakis, A. F., 2014, "Realization of a Strongly Nonlinear Vibration-Mitigation Device Using Elastomeric Bumpers," J. Eng. Mech., **140**(5), p. 04014009.
[24] Luo, J., Wierschem, N. E., Fahnestock, L. A., Spencer, B. F., Jr., Quinn, D. D., McFarland, D. M., Vakakis, A. F., and Bergman, L. A., 2014, "Design,

Simulation, and Large-Scale Testing of an Innovative Vibration Mitigation Device Employing Essentially Nonlinear Elastomeric Springs," Earthquake Eng. Struct. Dyn., **43**(12), pp. 1829–1851.
[25] Wierschem, N. E., Hubbard, S. A., Luo, J., Fahnestock, L. A., Spencer, B. F., Jr., McFarland, D. M., Quinn, D. D., Vakakis, A. F., and Bergman, L. A., 2017, "Response Attenuation in a Large-Scale Structure Subjected to Blast Excitation Utilizing a System of Essentially Nonlinear Vibration Absorbers," J. Sound Vib., **389**, pp. 52–72.
[26] Kittel, C., 1996, *Introduction to Solid State Physics*, 7th ed., John Wiley and Sons, New York.
[27] Kim, E., Li, F., Chong, C., Theocharis, G., Yang, J., and Kevrekidis, P. G., 2015, "Highly Nonlinear Wave Propagation in Elastic Woodpile Periodic Structures," Phys. Rev. Lett., **114**(11), p. 118002.
[28] Sugino, C., Leadenham, S., Ruzzene, M., and Erturk, A., 2016, "On the Mechanism of Bandgap Formation in Locally Resonant Finite Elastic Metamaterials," J. Appl. Phys., **120**(13), p. 134501.
[29] Narisetti, R. K., Leamy, M. J., and Ruzzene, M., 2010, "A Perturbation Approach for Predicting Wave Propagation in One-Dimensional Nonlinear Periodic Structures," ASME J. Vib. Acoust., **132**(3), p. 031001.